Influence of the porphyrin structure and linker length on the interfacial behavior of phospholipid-porphyrin conjugates

Louis-Gabriel Bronstein, Paul Cressey, Wasim Abuillan, Oleg Konovalov, Maciej Jankowski, Véronique Rosilio, Ali Makky

Influence of the porphyrin structure and linker length on the interfacial behavior of phospholipid-porphyrin conjugates

Louis-Gabriel Bronstein[a], Paul Cressey[a], Wasim Abuillan[b], Oleg Konovalov[c], Maciej Jankowski[c], Véronique Rosilio[a] and Ali Makky[a] *

[a] Université Paris-Saclay, CNRS, Institut Galien Paris-Saclay, 92296, Châtenay-Malabry, France

[b] Physical Chemistry of Biosystems, Physical Chemistry Institute, University of Heidelberg, 69120 Heidelberg, Germany

[c] European Synchrotron Radiation Facility (ESRF), Grenoble, 38043, France

* Corresponding author: ali.makky@universite-paris-saclay.fr

ABSTRACT

Hypothesis: Phospholipid-porphyrin (Pl-Por) conjugates consist of porphyrin derivatives grafted to a lysophosphatidylcholine backbone. Owing to their structural similarities with phospholipids, Pl-Por conjugates can self-assemble into liposome-like assemblies. However, there is a significant lack of information concerning the impact of the porphyrin type and the length of the alkyl chain bearing the porphyrin on the interfacial behavior of the Pl-Por conjugates. We hypothesized that changing the chain length and the porphyrin type could impact their two-dimensional phase behavior and modulate the alignment between the two chains.

Experiments: 6 Pl-Por conjugates with different alkyl chain lengths in the sn2 position of C16 lysophosphatidylcholine and coupled to either pheophorbide-a or pyropheophorbide-a were synthesized. Their interfacial behavior at the air/water interface was assessed using Langmuir balance combined to a variety of other physical techniques including Brewster angle microscopy, atomic force microscopy and X-ray reflectometry.

Findings: Our results showed that all 6 Pl-Por form stable monolayers with the porphyrin moiety at the air/water interface. We also showed that changing the porphyrin moiety controlled the packing of the monolayer and thus the formation of organized domains. The chain length dictated the structure of the formed domains with no evidence of the alignment between the two chains.

KEYWORDS

Phospholipid-porphyrin conjugate; monolayer; X-ray reflectometry; Atomic force microscopy; Langmuir-Blodgett film.

1. Introduction

Porphyrins and their derivatives are the most abundant pigments in nature [1-2]. These ubiquitous macrocycles play a vital role in many biological functions such as photosynthesis, oxygen transport, oxygen storage [3] and cell respiration [1]. In addition, many porphyrin derivatives have been used as photosensitizers in photodynamic therapy which is considered an efficient and minimally invasive treatment modality for both cancer and local bacterial infections [2, 4]. Moreover, grafting porphyrin derivatives to a lipid backbone such as lysophosphatidylcholine (LPC) led to phospholipid-porphyrin (Pl-Por) conjugates [5-6] that were shown to self-assemble into liposome-like nanostructures named "porphysomes" [7] thanks to their phospholipid structure and the intermolecular interactions between the grafted porphyrins. These assemblies possess unique optical and photophysical properties [7-8] compared to their monomeric counterparts or to the unconjugated porphyrins. Indeed, depending on the porphyrin derivative, porphysomes show an intensive red-shift of the Q_y-absorption band due to the formation of well-organized porphyrins aggregates called J-aggregates [9-11]. The dense packing of porphyrin molecules within these nanostructures provokes an intense fluorescence quenching of the porphyrin chromophores. Upon their illumination, the absorbed photonic energy usually

released as fluorescence and singlet oxygen is dissipated thermally through vibrational relaxation [7]. Therefore, the nanoassemblies may act as highly efficient cytotoxic photothermal agents and can be used in photothermal therapy. Interestingly, once the porphysomes have been passively disrupted in the body, both the fluorescence and photosensitizing properties of the porphyrin pigments are regenerated thus enabling their photodynamic properties. Consequently, Pl-Por conjugates are nowadays considered as versatile building blocks for the conception of multifunctional nanomaterials for several biomedical applications [7, 12-16] including photothermal therapy, photodynamic therapy, photo-triggered drug release, fluorescence and photoacoustic imaging [7]. The Pl-Por conjugates that have been described so far for biomedical applications were usually synthesized through esterification of the sn-2 position of lysophosphatidylcholine with either pyropheophorbide-a (Pyro-a) [7] or bacteriochlorophyll a [7]. Other conjugates with benzoporphyrin derivative [15-16] have also been reported for photodynamic therapy applications. However, despite the versatility of these conjugates, there is a significant lack of information concerning their interfacial behavior. Studying the interfacial behavior of these compounds would offer a better understanding on how these compounds interact with each other and what conformation they adopt at the interface which in turn may give answers about the impact of the chemical structure on their assembling properties. In previous work we synthesized two lipid-porphyrin conjugates that were obtained by coupling pheophorbide-a (Pheo-a) [17] to either lyso-sphingomyelin (PhLSM) or a modified lyso-phosphatidylcholine with a C6 alkyl chain length linker in sn2 position (Ph_6LPC, n=5) [5-6, 18]. Their interfacial behavior at the air/water interface and self-assembling efficiency in aqueous medium were characterized [5-6, 18]. Our results demonstrated that both conjugates were able to self-assemble into liposome-like structures in buffer, but these assemblies were unstable with time. By combining Langmuir balance with X-ray reflectometry, we demonstrated that Ph_6LPC

formed a thicker monolayer with a higher electron density in the alkyl chains region than that of PhLSM. This was explained by a conformational difference between the two compounds. For Ph_6LPC, the Pheo-a moiety aligns with the sn2 C16 alkyl chain whereas for PhLSM it remains at the interface near the polar head group. The instability of these nanoassemblies was interpreted as the result of a mismatch between the length of the alkyl chain in sn-1 position and the adjacent porphyrin, leading to an inadequate packing parameter for bilayer stability [5-6]. However, since the lipid backbones in PhLSM and Ph_6LPC conjugates were structurally very different, a clear conclusion about the effect of the chemical structure on their assembling and interfacial properties could not be drawn. Here, we specifically focus on addressing the impact of i) the length of the chain separating the porphyrin from the polar headgroup and ii) the type of porphyrin on the interfacial behavior of Pl-Por conjugates. In this aim, we synthesized two new series of Pl-Por conjugates exhibiting different alkyl chain lengths in sn2 position and linked to either pheophorbide-a [17] (Ph_xLPC) or pyropheophorbide-a [7] (Pyr_xLPC) via amide coupling (Figure 1). Our motivation for changing the length of the linker in sn2 position is to reduce the chain length mismatch between the sn1 and sn2 alkyl chains. Moreover, changing the porphyrin structure could play an important role in the interaction between the conjugates at the interface and influence molecules packing. Herein, the synthesized conjugates were characterized as monolayers at the air/water interface using a Langmuir balance. The morphology of the monolayers was thoroughly studied using Brewster angle microscopy (BAM) and atomic force microscopy (AFM) on Langmuir-Blodgett transferred films. In addition, the fine structure normal to the interface was studied by X-ray reflectometry (XRR).

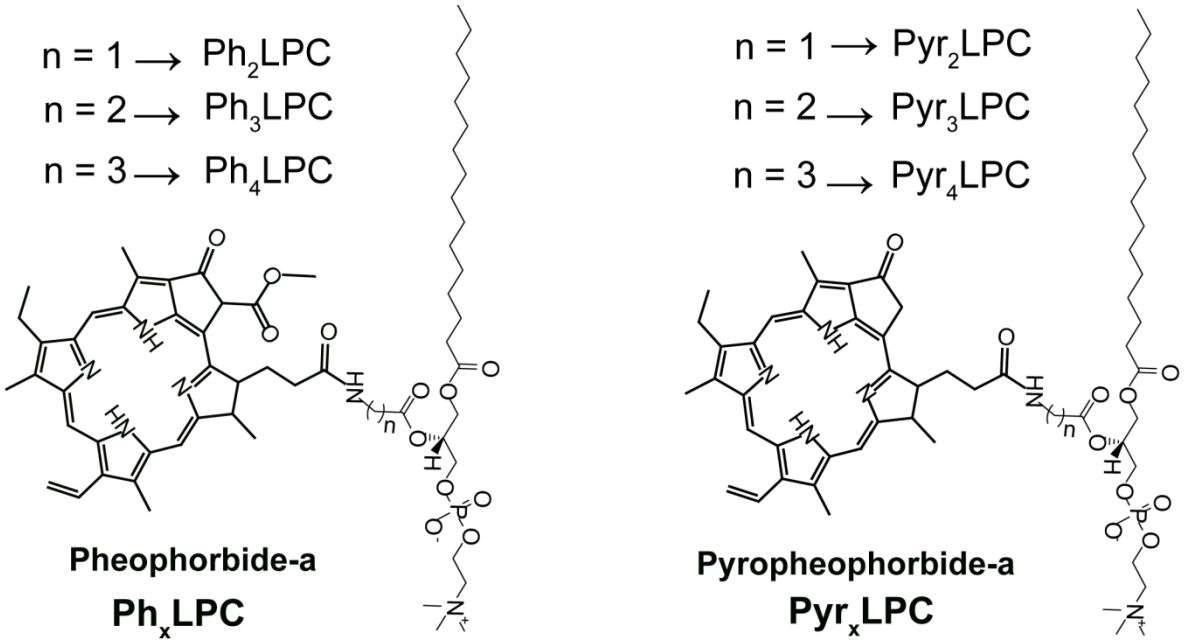

Figure 1: Structure of lipid-porphyrin conjugates Ph_xLPC and Pyr_xLPC bearing pheophorbide-a and pyropheophorbide-a chromophores, respectively.

2. Material and methods

2.1. Chemicals

Pheophorbide-a (Pheo-a, ≥ 95%, mixture of diastereomers, Mw = 592.69 g/mol) and pyropheophorbide-a (Pyro-a, ≥ 95%, Mw = 534.66 g/mol) were purchased from Livchem Logistics GmbH (Frankfurt, Germany). 1-palmitoyl-2-hydroxy-sn-glycero-3-phosphocholine (16:0 Lyso-PC, 99%, Mw = 495.63 g/mol) and 1,2-dipalmitoyl-sn-glycero-3-phosphocholine (16:0 PC (DPPC), 99%, Mw = 734.04 g/mol) were purchased from Avanti Polar Lipids (Alabaster, AL). The ultrapure water (γ = 72.2 mN/m at 22° C) used in all experiments was produced by a Millipore Milli-Q® Direct 8 water purification system, with a resistivity of 18.2 MΩ.cm. Solvents were purchased from CARLO ERBA Reagents (Val de Reuil, France). All compounds and solvents were used without further purification.

2.2. Synthesis of lipid-porphyrin conjugates

Ph_xLPC and Pyr_xLPC were synthesized as described previously [5] with some modifications as shown in the Figure S1. The modified phospholipids were synthesized by conjugating the corresponding *tert*-butyloxycarbonyl (BOC)-protected linker to the secondary alcohol in sn2 position of the 1-lysophosphatidylcholine backbone via direct acylation of the carboxylate group. This acylation was carried out following a modified procedure outlined by Rosetto et al.[19-21]. In brief, the reaction mixture was sonicated at 25°C in the presence of glass beads, under basic conditions using 1-Ethyl-3-(3′-dimethylaminopropyl)carbodiimide·HCl (EDC.HCl) to activate the carboxylic acid. The BOC protected amine was deprotected under acidic conditions using HCl:dioxane. Following the deprotection, the attachment of pheophorbide-a or pyropheophorbide-a was carried out following regular amide coupling reaction conditions using EDC.HCl/ 1-hydroxybenzotriazole (HOBt) as the coupling agents. The resulting procedure gave 6 different conjugates classified in two series: Pyr_xLPC was composed of Pyr_2LPC (yield 45% MALDI for $[C_{59}H_{85}N_6O_{10}P]^+$; calculated: 1068.62 g.mol^{-1} $[M+H]^+$; observed: 1069.64 g.mol^{-1}), Pyr_3LPC (yield 72% MALDI for $[C_{60}H_{87}N_6O_{10}P]^+$; calculated: 1082.62 g.mol^{-1} $[M+H]^+$; observed: 1083.67 g.mol^{-1}) and Pyr_4LPC (yield 44% MALDI for $[C_{61}H_{89}N_6O_{10}P]^+$; calculated: 1096.64 g.mol^{-1} $[M+H]^+$; observed: 1097.69 g.mol^{-1}). Ph_xLPC consisted of Ph_2LPC (yield 38% MALDI for $[C_{61}H_{87}N_6O_{12}P]^+$; calculated: 1126.63 g.mol^{-1} $[M+H]^+$; observed: 1127.64 g.mol^{-1}), Ph_3LPC (yield 42% MALDI for $[C_{62}H_{89}N_6O_{12}P]^+$; calculated: 1140.64 g.mol^{-1} $[M+H]^+$; observed: 1141.62 g.mol^{-1}) and Ph_4LPC (yield 33%, MALDI for $[C_{63}H_{91}N_6O_{12}P]^+$; calculated: 1176.64 g.mol^{-1} $[M+H]^+$; observed: 1177.64 g.mol^{-1}).

2.3. Surface pressure measurements

Surface pressure-surface area isotherms of the pure components were recorded using a thermostated KSV-Nima Langmuir film balance (Biolin Scientific, Finland), composed of a Teflon trough (775.75 cm^2) equipped with two 145 mm long Delrin barriers. The free porphyrins and their conjugates in chloroform/methanol (9:1) solutions were spread (~5×10^{16} to 6×10^{16} molecules) onto aqueous HEPES buffer solution (10 mM HEPES, 150 mM NaCl, pH = 7.4). After deposition, the solvents were left to evaporate for 15 min before compression of the monolayer at a rate of 10 $Å^2$/molecule/min. All experiments were performed at 22±1 °C and the results reported are mean values of at least three measurements. From the surface pressure−area data, the surface compressional moduli (K) of monolayers were calculated, using Eq. 1 with A the molecular area and π, the surface pressure:

$$K = -A\left(\frac{\partial \pi}{\partial A}\right)_T \qquad \textit{(Eq. 1)}$$

2.4. Brewster angle microscopy (BAM)

The morphology of the lipid-porphyrin monolayers at the air/water interface was monitored using a Brewster angle microscope (Micro-BAM 3, NimaTechnology Ltd, Coventry, UK) mounted on a Langmuir trough. The microscope was equipped with a frequency laser diode (λ = 659 nm, 30 mW optical power) generating a collimated beam of approximately 6 mm diameter, with a p-polarizer, analyzer, and a USB camera. The refracted beam was absorbed by a black glass plate placed in the subphase. The field of view of BAM was 3.6 × 4.1 mm^2. The image size was rescaled and the zone of interest was cropped using imageJ software to get a final image size of 2.0 × 2.0 mm^2 with a resolution of 5.6 µm/pixel.

2.5. Langmuir-Blodgett transfer and atomic force microscopy (AFM) imaging

The Langmuir–Blodgett (LB) film transfer of the lipid-porphyrin monolayers was performed on freshly cleaved mica surfaces (1.5 × 1.5 cm^2) using the Langmuir trough equipped with a Teflon well. The freshly cleaved mica substrate was immersed into the buffer subphase, and then the corresponding lipid-porphyrin conjugate solution was spread (total number of spread molecules ~ 5×10^{16}) onto the subphase. After solvent evaporation, the monolayer was compressed at a constant rate (10 $Å^2$/molecule/min) and the pressure-area (π-A) isotherm was simultaneously recorded. When the desired surface pressure was reached, it was maintained constant and the mica substrate (1.5×1.5 cm^2) was lifted from the subphase at a speed of 1 mm/min. Afterwards, atomic force microscopy (AFM) imaging of the transferred lipid-porphyrin films was performed in ambient conditions at room temperature using a JPK Nanowizard Ultraspeed atomic force microscope from JPK Instruments (Berlin, Germany) in amplitude modulation AFM (AM-AFM) with force settings comprised between 55–65% of the free amplitude A ~12 nm). Gold-coated silicon SCOUT-350 cantilevers (nominal spring constant ~ 42 nN/nm, resonant frequency ~ 350 KHz, conical shape tip radius <10 nm) from NuNano (Bristol, UK) were used. For each transferred film, different regions of the mica substrate were systematically imaged at high resolution (5× 5 μm^2, 10 x 10 μm^2 and 15 × 15 μm^2 at 1024 x 1024 pixels) with the AFM. AFM images were processed using the JPK-SPM Data Processing software (version 6.1.131). All AFM images were flattened by subtracting a polynomial fit from each scan line at a 2^{nd} regression order. For the orientation determination of the imaged objects, the processed AFM images were saved as grayscale images. The grayscale AFM images were then analyzed using OrientationJ [22] which is an imageJ plug-in. We choose the "OrientationJ Analysis" option and the "Cubic Spline" function [22] to compute the gradient. The structure tensor was set to 3 pixels which corresponds to the width of the smallest fibril.

2.6. X-ray reflectivity experiments at the air/buffer interface

XRR experiments were carried out at the beamline ID10 of the European Synchrotron Radiation Facility (ESRF, Grenoble, France). The samples were irradiated with a monochromatic synchrotron beam with an energy of 8 keV (λ = 1.55 Å). The XRR experiments were performed on monolayers of lipid-porphyrin conjugates spread on the surface of HEPES buffer (HEPES 10 mM, NaCl 150 mM, pH 7.4) and compressed to a surface pressure of 30 mN/m. The film balance was kept in a helium atmosphere to minimize air scattering and maintain a consistent environment for each measurement. XRR was measured with a MAXIPIX 2D detector (Multichip Area X-ray detector based on a photon-counting Pixel array) [23]. The error bars in the XRR curves correspond to the error resulting from the counting statistics and were calculated as described previously [24]. After background subtraction, the specular reflectivity was analyzed using a genetic minimization algorithm implemented in the MOTOFIT software package [25] by choosing a two-slab model (see supporting information).

3. Results

3.1. Surface pressure measurements

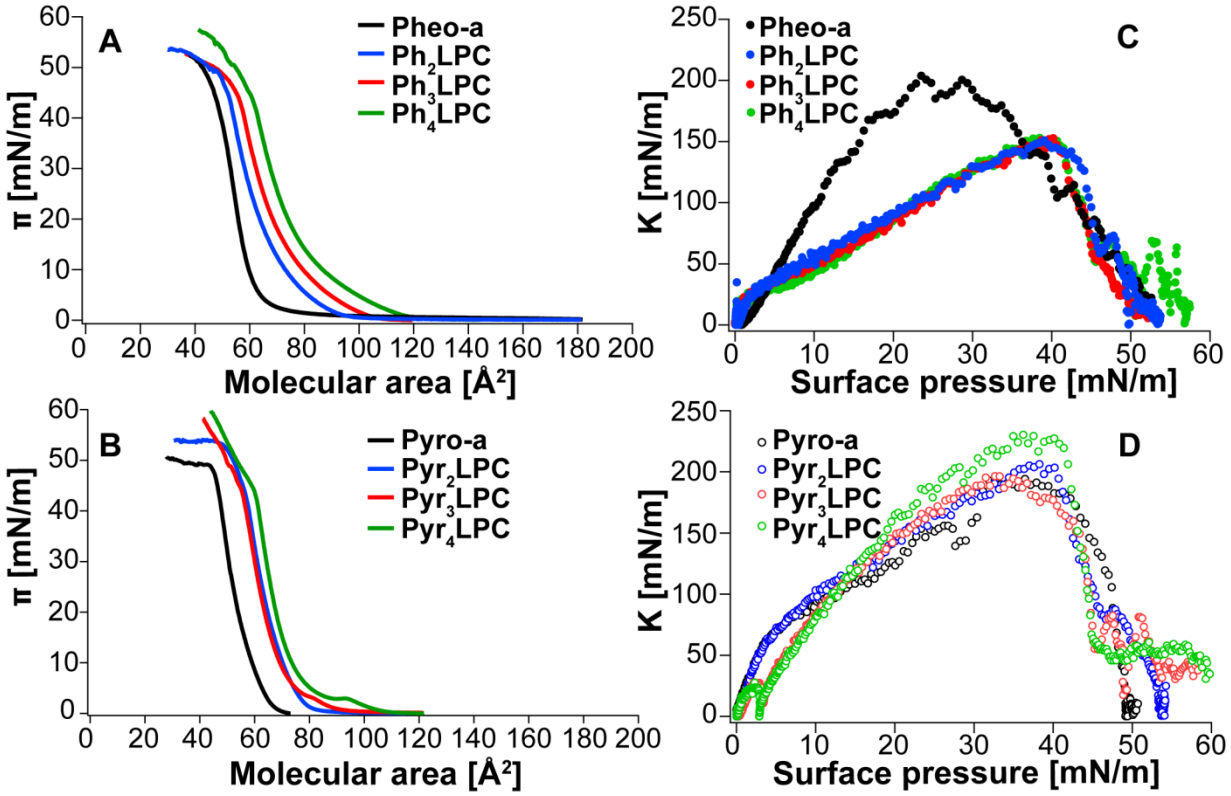

Figure 2: π-A isotherms (A, B) and the corresponding compressibility modulus (C, D) for pheophorbide-a and pyropheophorbide-a derivatives spread on HEPES buffer at 22±1°C.

To assess the impact of the porphyrin type and the spacer length on the interfacial behavior of the two series of lipid porphyrin-conjugates, we compared the molecular organization of the conjugates and unmodified porphyrins spread at the air/buffer interface, using the Langmuir film balance. The π-A isotherms obtained for the two porphyrins (Pheo-a and Pyro-a) and the two synthesized lipid-porphyrin conjugates series (Ph_xLPC and Pyr_xLPC) are shown in Figure 2. To compare the features of these isotherms, we estimated the molecular area at the surface pressure onset also named lift-off area (A_0) and the limit area (A_{limit}) which is obtained from the zero intersection by extrapolating the linear steep increase of the surface pressure [26-27]. The compressibility modulus (K) was also determined. These parameters are summarized in Table 1.

Pheo-a exhibited similar isotherm characteristics as reported previously [5] with $A_0 \sim 80$ Å^2 and $A_{limit} \sim 60$ Å^2. This corresponds to a side-on orientation of the Pheo-a molecules exposing their carboxylic and ester groups to the buffer subphase with subsequent formation of closely packed films of Pheo-a molecules [5].

Comparing the Ph_xLPC isotherms with that of the parent Pheo-a molecule, it can be readily seen that all Ph_xLPC compounds show similar isotherm shapes but form more expanded monolayers (Table 1). Moreover, the isotherms exhibit a monotonic shift toward larger molecular areas as the length of the spacer separating the polar headgroup from Pheo-a increases. Ph_3LPC and Ph_4LPC exhibit an increase in the molecular area at the surface pressure onset (A_0) of 9 % and 26 %, respectively compared to Ph_2LPC which possesses the shortest spacer. Besides, the maximal compression modulus (K_{max}) values for PhxLPC ($K_{max} \sim 150$ mN/m) are lower than those for Pheo-a monolayer ($K_{max} \sim 220$ mN/m). Such behavior could be explained by the presence of the PC polar head group with the acyl chain bearing Pheo-a at the interface which enlarge the molecular area of the Ph_xLPC compounds and hinder the close packing of Pheo-a molecules, resulting in a compression modulus reduction. It is worth noting that the differences between the molecular areas of Ph_xLPC conjugates remain constant up to the collapse unlike the previously synthesized Ph_6LPC compounds with longer spacer (n = 5) [5]. This suggests that the Pheo-a molecule attached to the lipid backbone remains at the interface even at high surface pressure without re-alignment with the sn-1 C16 alkyl chain or looping of the Pheo-a conjugated acyl chain toward the buffer subphase [5]. The shorter spacer length provides less flexibility for the attached porphyrin core to adopt distinct local orientations at different surface pressures.

Like Ph_xLPC compounds, the surface pressure onset for the Pyr_xLPC series are larger than the unconjugated chromophore (Pyro-a). Pyro-a displays a similar isotherm to Pheo-a but with

slightly smaller A_{onset} and A_{limit} values, ~ 76 $Å^2$ and 58 $Å^2$, respectively. This slight reduction of 3 $Å^2$ in the molecular area of Pyro-a compared to Pheo-a is most likely due to the absence of the methyl ester group on the porphyrin ring thus reducing the volume of the porphyrin hydrophilic group. The π-A isotherms of Pyr_xLPC compounds show A_{onset} values of ~ 80 $Å^2$, 93 $Å^2$ and 108 $Å^2$ for Pyr_2LPC, Pyr_3LPC and Pyr_4LPC respectively, all larger than that of the Pyro-a alone. Here again, the enlargement of the A_{onset} is consistent with the increasing length of the linker from Pyr_2LPC to Pyr_4LPC, suggesting the effect of presence of the Pyro-a at the interface. However, while the Ph_xLPC compounds display a monotonic increase in the surface pressure during monolayer compression with expanded-like profile, a slight plateau-like region appears for Pyr_3LPC and Pyr_4LPC isotherms at surface pressures of ~ 2-3 mN/m. Such behavior is usually observed with phospholipids such as DPPC where liquid-expanded (LE) and liquid-condensed (LC) states coexist during the first-order phase transition between the two monolayer states [28-29]. Interestingly, the plateau-like pressure of Pyr_3LPC and Pyr_4LPC increases with subsequent reduction of the plateau region when the temperature of the buffer subphase is augmented from 17°C to 29°C (Figure S2). This confirms that the plateau-like region originates from the coexistence of the LE and LC states. Surprisingly, the isotherm of the Pyr_2LPC with the shorter spacer length does not display any plateau-region. Moreover, while the grafting of Pyro-a to the sn2 chains of the modified lipids induces larger A_{onset}, A_{limit} does not seem to be significantly affected by the spacer length. Thus, Pyr_xLPC may adopt similar molecular packing at high surface pressures independently of the linker length. Unlike monolayers of Ph_xLPC compounds showing lower compression modulus than those of pure Pheo-a, Pyr_xLPC ones display similar maximal compression modulus (K_{max}~200 mN/m) as Pyro-a. These monolayers are in the liquid condensed state [30]. This indicates that the grafting of Pyro-a on the sn2 chains via different

spacer length does not affect the lateral packing of the Pyro-a molecules at the air/water interface and thus the monolayer rigidity.

Table 1: Molecular area at surface pressure onset (A_0), molecular area at surface pressure of 30 mN/m (A_{30}), limit molecular area (A_{limit}), and maximal compressional modulus (K_{max}) for Pheo-a, Ph_xLPC, Pyro-a and Pyr_xLPC monolayers. The reported values are the average ± standard deviation of n = 3 independent experiments.

Monolayer composition	**A_0 (Å^2)**	**A_{30} (Å^2) at 30 mN/m**	**A_{limit} (Å^2)**	**K_{max} (mN/m)**
Pheophorbide-a	79±4	51±3	60±4	220±34
Ph_2LPC	95±2	57±2	74±2	145±13
Ph_3LPC	104±2	63±2	77±2	148±7
Ph_4LPC	120±1	66±1	81±2	158±12
Pyropheophorbide-a	76±2	50±1	58±1	190±13
Pyr_2LPC	80±3	61±1	71±1	208±6
Pyr_3LPC	93±1	61±1	70±2	222±39
Pyr_4LPC	108±2	64±1	74±2	250±36

3.2. Brewster angle microscopy analysis

To further investigate the different states of lipid-conjugates monolayers, Brewster angle microscopy (BAM) images were recorded at increasing surface pressures (Figure 3). Monolayers of Ph_xLPC compounds appear homogenous and smooth, which confirms the LE state deduced from their isotherms and compression modulus values. Conversely, monolayers of Pyr_xLPC compounds exhibit bright domain-like structures even before the surface pressure starts to rise (*i.e.* 0 mN/m) and change morphology upon further monolayer compression. The bright domains observed for Pyr_2LPC grow gradually with monolayer compression to form homogeneous stratified monolayer at 1 mN/m. The Pyr_4LPC monolayer shows similar morphology, but with smoother aspect at surface pressures between 1 and 5 mN/m. Interestingly, the Pyr_3LPC monolayer exhibits different features during molecular compression at the air/buffer interface. Added to the homogeneous bright domains observed for the other two Pyr_xLPC compounds, the

Pyr_3LPC monolayer displays supramolecular rod-like structures at a surface pressure of 0 mN/m, and their number increases when the surface pressure increases up to 10 mN/m.

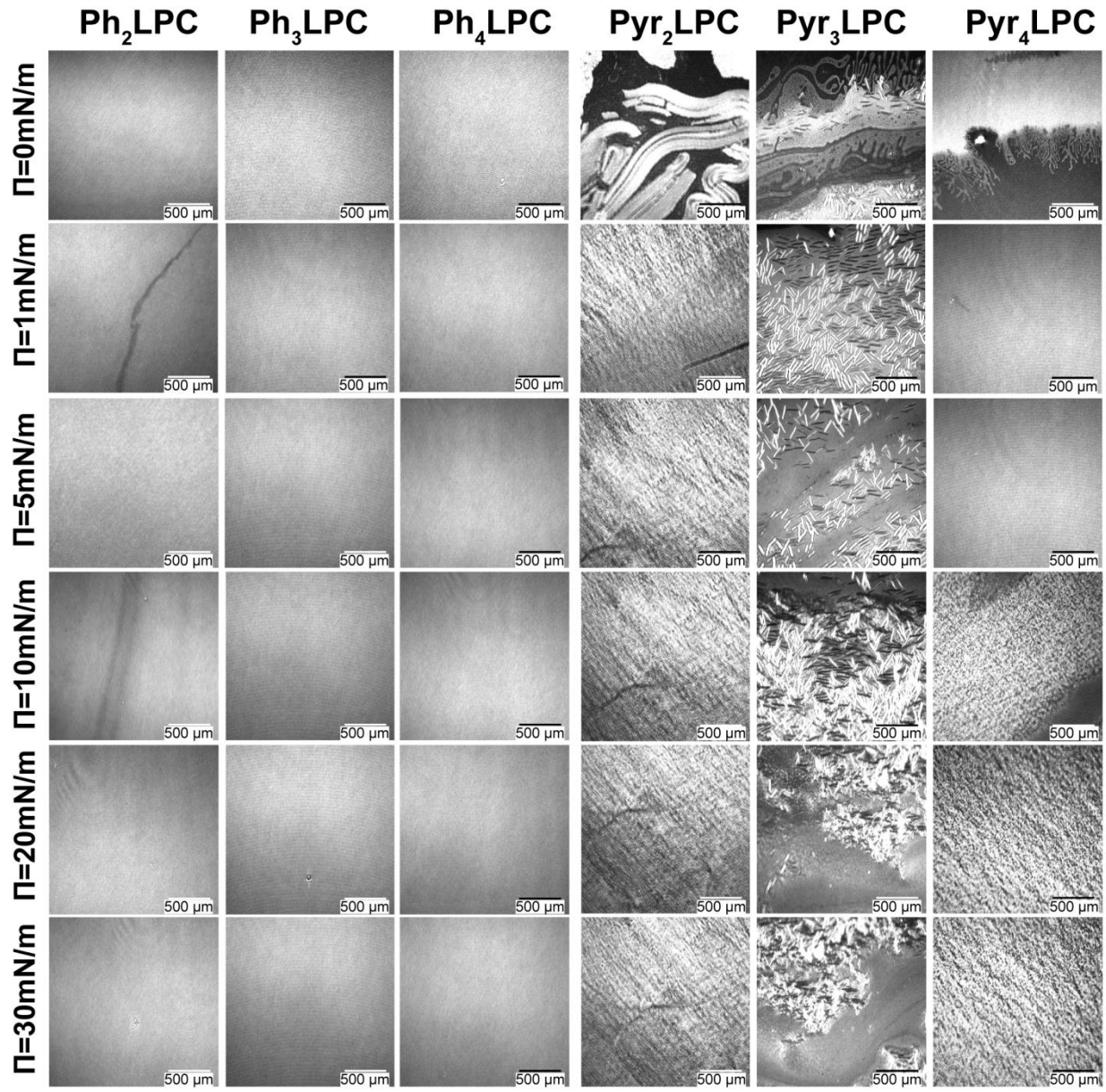

Figure 3: Representative BAM images recorded during compression of Ph_xLPC and Pyr_xLPC monolayers spread on HEPES buffer at 22±1°C. The scale bar corresponds to 500 µm.

It should be noticed that some of these rod-like structures appear dark. This implies that these structures are 3D in shape and possess an inner anisotropy. In other words, the observation of dark or bright structures arises from the relative orientation of the rod-like supramolecular

structures at the interface relative to the incident p-polarized laser. At a surface pressure of 10 mN/m, the rods get close to each other and collapse at higher surface pressures. The Pyr_3LPC monolayer shows the coexistence of both smooth condensed monolayers and 3D rod-like structures even at a surface pressure of 30 mN/m. These observations suggest that Pyr_3LPC do not form homogenous monolayer but rather 3D rod like structures mixed with a 2D condensed monolayer.

3.3. AFM assessment of the conjugates' domains morphology

BAM enables the detection of microdomains that grow upon compression at the air/water interface, however due to its resolution limit, it does not allow the visualization of the nanodomains or the structure of the nuclei that may form during monolayer compression. Thus, the monolayers of the various lipid-porphyrin conjugates studied were transferred at a surface pressure of 30 mN/m onto mica substrates by the Langmuir-Blodgett technique and then, they were imaged by AFM in air conditions (Figure 4). While the topographic AFM images of Ph_xLPC films (Figure 4, upper panel) show smooth homogenous monolayers confirming the absence of structured domains, Pyr_xLPC films exhibit domains with different shape depending on the spacer length (Figure 4, lower panel). Pyr_2LPC compound forms a stratified monolayer with the presence of condensed domains that are consistent with BAM images (Figure 3). In the case of Pyr_3LPC and Pyr_4LPC, elongated structures are observed with lengths of several micrometers and maximal width up to 1 µm. It should be noticed that Pyr_3LPC forms wider and relatively shorter domains than Pyr_4LPC.

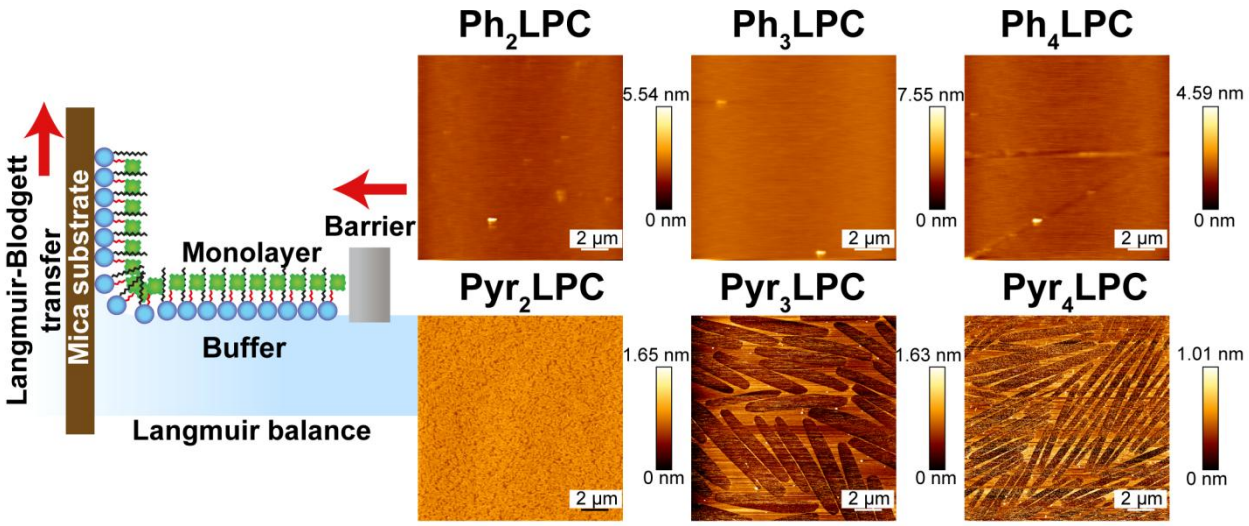

Figure 4: Schematic illustration of the Langmuir-Blodgett technique used to transfer the compounds onto mica substrates (left). AM-AFM topography images of Ph_xLPC and Pyr_xLPC compounds transferred at a surface pressure of 30 mN/m (right).

In order to get a better understanding on the formation of these elongated domains for Pyr_3LPC and Pyr_4LPC, Langmuir-Blodgett films were transferred onto mica substrates at surface pressures near the plateau-like region (π = 2 mN/m, Figure 5) and above the transition (π = 15 mN/m, Figure 6). The transferred Pyr_3LPC film at 2 mN/m shows the appearance of nucleated molecules into well-defined structures (Figure 5A) with both straight fibrils-like and tape-like structures, with average heights of ~ 1.5 nm and ~ 2.0 nm, respectively. It is worth noting that these fibrils and tape-like structures have a specific orientation. While the fibrils are oriented toward the same direction, tape-like ones are aligned at an angle of 30 °C (Figures 5, B and C). In the case of Pyr_4LPC film, twisted fibril-like structures of ~ 1.5 nm in height are revealed with the presence of accumulated branched structures (Figures 5D-F).

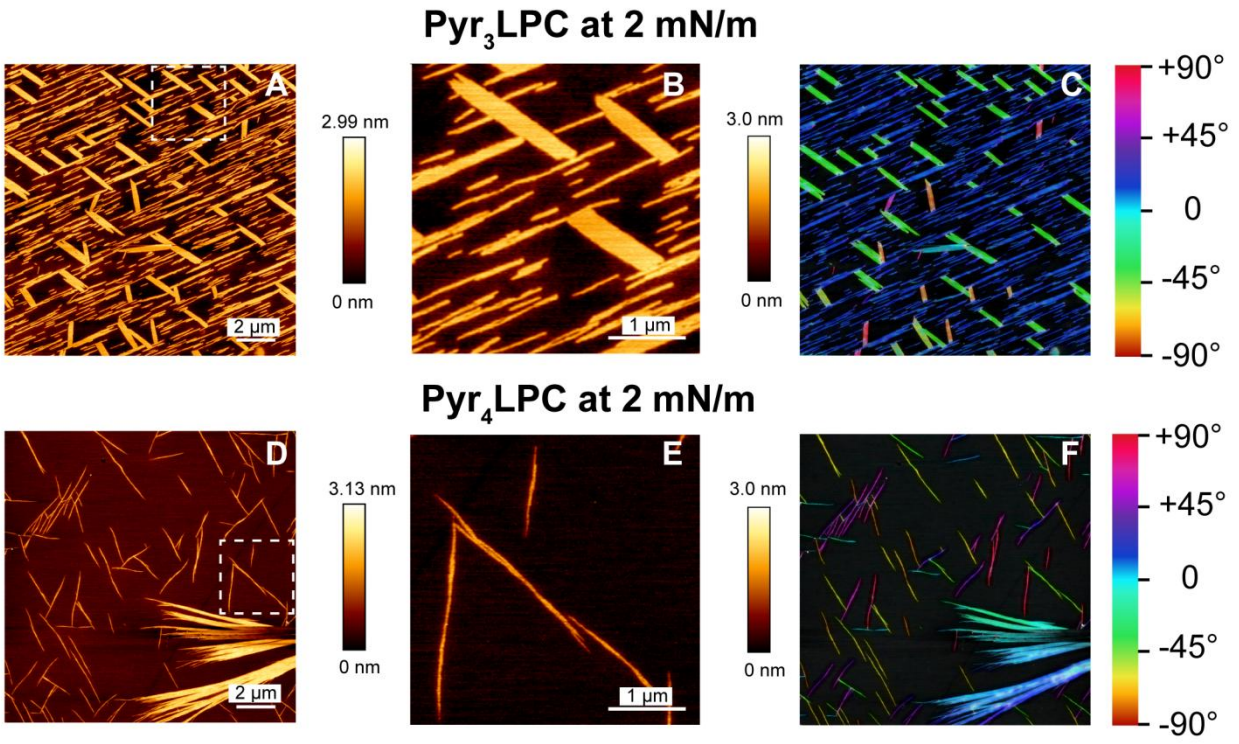

Figure 5: AM-AFM topography images of (A, B) Pyr_3LPC and (D, E) Pyr_4LPC compounds transferred on mica substrate at a surface pressure of 2 mN/m. The results of the features orientation were determined using OrientationJ[22], ImageJ plug-in which allowed getting HSB (Hue-Saturation-Brightness) color-coded maps (C, F) for Pyr_3LPC and Pyr_4LPC, respectively.

At the surface pressure of 15 mN/m, the transferred Pyr_3LPC monolayers show very long tape-like structures of several micrometers long, 2-3 µm wide with an average height of ~ 2 nm (Figure 6A). Surprisingly, some regions also show 3D rod-like structures of ~ 25 nm high (Figure 6B) indicating the presence of piling up of these elongated structures. The compression of Pyr_4LPC monolayer up to 15 mN/m results in the formation of similar elongated structures with ~1.5 nm height and several micrometers in length (Figure 6C). In addition, Pyr_4LPC shows similar structure shape with an average height of ~10 nm in some regions (Figure 6D). However, they are narrower than those observed in the Pyr_3LPC films and show a shallow groove throughout the rod. Thus, both Pyr_3LPC and Pyr_4LPC compounds can self-assemble into rod-like structures at the air/water interface with clear evidence that the linker length has an impact on the morphology of the rods.

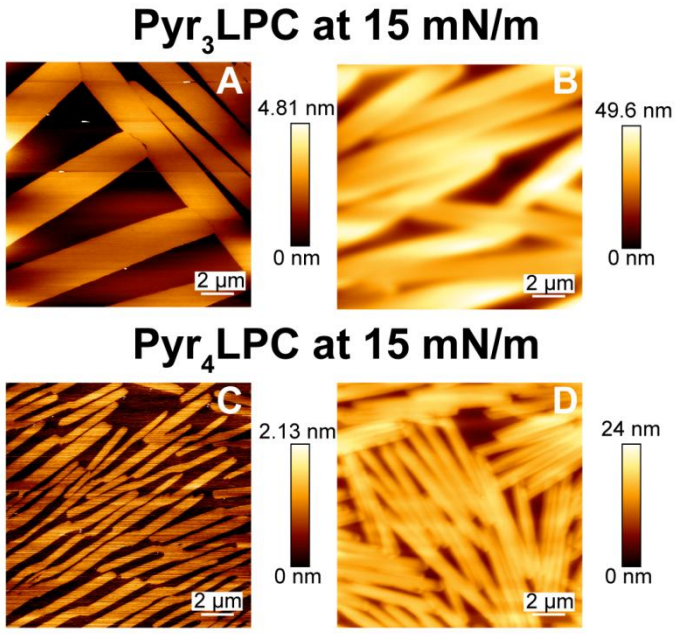

Figure 6: AM-AFM topography images of Pyr_3LPC (A, B) and Pyr_4LPC (C, D) compounds transferred on mica substrate at a surface pressure of 15 mN/m.

3.4. Fine structures of PL-Por conjugate monolayers

The fine structures perpendicular to the plane of Ph_xLPC and Pyr_xLPC monolayers were studied using specular X-ray reflectivity (XRR). A monolayer of dipalmitoyl phosphatidylcholine (DPPC), a phospholipid with similar polar headgroup (i.e., choline headgroup) and alkyl chain length (16 carbons), was compressed to 30 mN/m and characterized by XRR for the sake of comparison. Figures 7A and 7B, show the XRR curves of DPPC, Ph_xLPC and Pyr_xLPC monolayers, fitted using a two-slab model. The corresponding electron density profiles (ρ) reconstructed from the best fit results (solid black lines in Figures 7A-B) along the z-axis are also shown in Figures 7C-D. The thickness (d), electron density (ρ) and root mean square roughness (σ) of each interface deduced from the best matching fits are summarized in Table 2. For the DPPC monolayer, the calculated total thickness is 24.2 Å, which agrees with literature values for

DPPC in the liquid condensed phase. Ph_xLPC monolayers have a total thickness of 16 to 17 Å depending on the spacer length. This 30 % difference in the total thickness of the Ph_xLPC monolayer compared to DPPC is most probably related to the difference in the packing density of the two compounds at 30 mN/m. Indeed, at this surface pressure, Ph_xLPC monolayers display larger molecular areas (57-66 $Å^2$) than DPPC (A_{30} = 48 $Å^2$). Thus, Ph_xLPC molecules are less ordered than DPPC ones where the two alkyl chains are aligned in the liquid condensed state. These thickness values are in good agreement with those estimated by AFM. The electron density of the hydrophobic regions of the Ph_xLPC monolayers (ρ_{HC} = 0.202-0.235 $e^-.Å^{-3}$) remains almost unchanged compared to DPPC (ρ_{HC} = 0.216 $e^-.Å^{-3}$) even though Ph_xLPC compounds possess only one alkyl chain per molecule and form more expanded monolayers than DPPC.

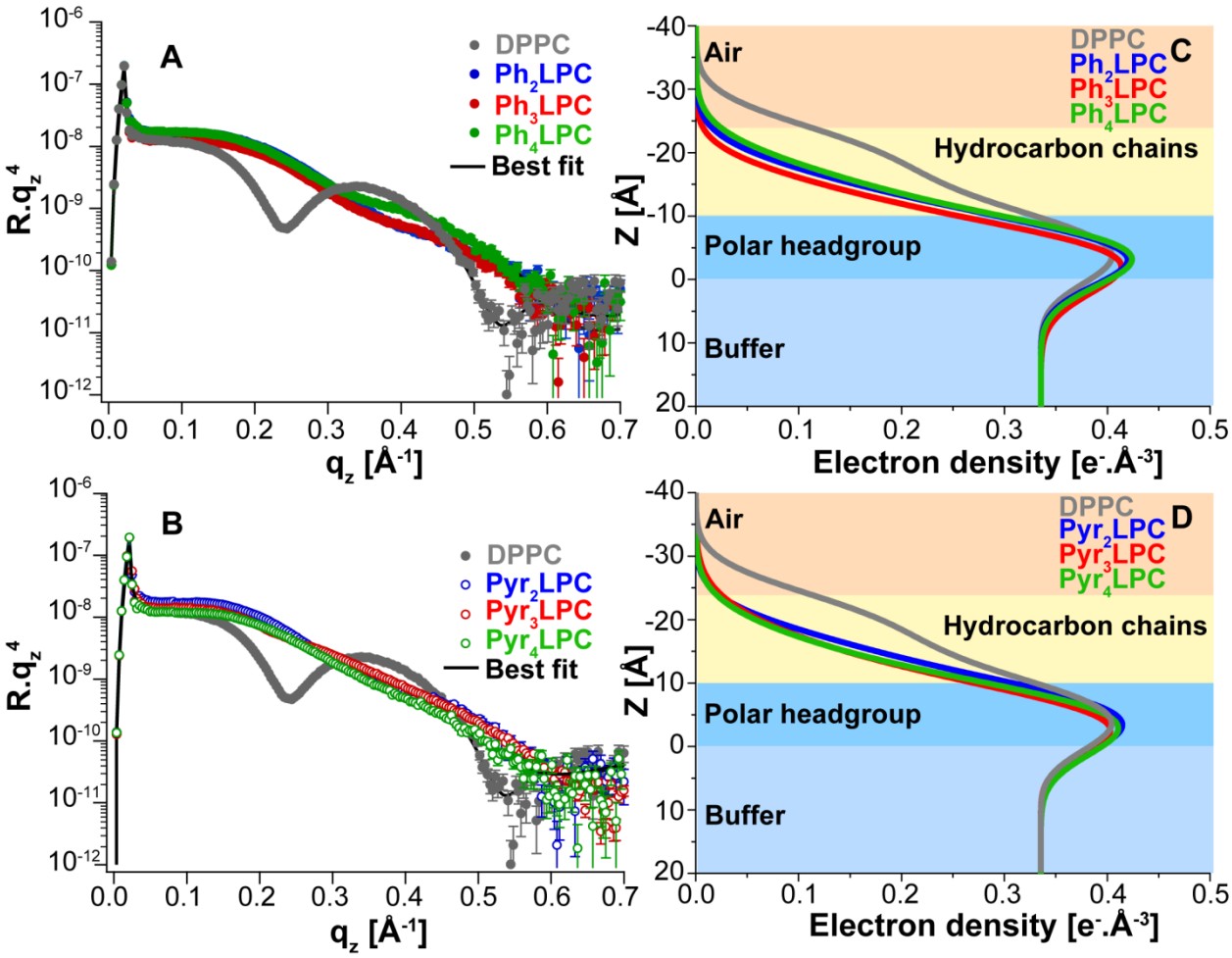

Figure 7: XRR curves of (A) Ph_xLPC and (B) Pyr_xLPC monolayers at a surface pressure of 30 mN/m. The solid lines represent the best model fits to the experimental data. Error bars for the reflectivity data represent the error resulting from the counting statistics. (C) and (D) are the reconstructed electron density profiles (e^- refers to the number of electrons) along the Z-axis for DPPC, Ph_xLPC and Pyr_xLPC compounds.

Conversely, the electron densities of the hydrophilic region (ρ_{polar} = 0.475-0.506 $e^-.Å^{-3}$) are significantly higher than that of the DPPC choline group ($\rho_{choline}$ = 0.418 $e^-.Å^{-3}$). Given that the total thickness of a Pheo-a monolayer is ~16 Å at 30 mN/m where the molecules take an upright orientation with respect to the interface, it is plausible that Pheo-a molecules remain at the air/water interface when conjugated to the modified phospholipids. This induces an increase in the electron density in both polar and hydrocarbon regions. Unlike the previously synthesized

Ph_6LPC compound (n = 5) [5], the spacer lengths for Ph_xLPC compounds (n=1, 2 or 3) are not long enough to allow the porphyrin core to align with the sn-1 C16 carbon chain. This result is in accordance with the isotherm's shape that remains expanded even at high surface pressures. A similar trend is observed for Pyr_xLPC monolayers, indicating that the latter molecules adopt similar conformations as those of Ph_xLPC. Again, the average thickness of Pyr_xLPC monolayers is consistent with AFM data, without indication of the presence of regions with 10-25 nm thicknesses. This is because XRR measures an ensemble average [31] (see supporting information) over few square millimeters indicating that thicker regions (> 2 nm) are less dominant (illumination area ~ 12-75 mm^2). It should be noted that the roughness of the hydrophobic region of Pyr_xLPC monolayers is increased by approximately 1 Å when compared to their Ph_xLPC counterparts. Such increase in the monolayer roughness is consistent with the formation of 2D and 3D domains in the monolayer as revealed by BAM and AFM experiments.

Table 2: Best fit parameters for the XRR Results for DPPC, Ph_xLPC and Pyr_xLPC monolayers at 30 mN/m as presented in Figure 7. The errors are the standard deviations resulting from the Gaussian error propagation during the refinement of the reflectivity curves. (e^- refers to the number of electrons)

	d (Å)	**ρ ($e^-.Å^{-3}$)**	**σ (Å)**
		DPPC	
Hydrophobic core	13.6±0.2	0.216±0.025	4.4±0.3
Choline group	10.6±0.4	0.418±0.016	4.4±0.5
Buffer	∞	0.335	3.3±0.2
		Ph_2LPC	
Hydrophobic core	8.5±0.2	0.202±0.014	4.8±0.2
Hydrophilic groups	7.5±0.3	0.506±0.014	4.7±0.4
Buffer	∞	0.335	4.1±0.4
		Ph_3LPC	
Hydrophobic core	8.6±0.2	0.207±0.011	4.9±0.1
Hydrophilic groups	8.3±0.2	0.481±0.006	4.2±0.1
Buffer	∞	0.335	4.0±0.1
		Ph_4LPC	
Hydrophobic core	8.6±0.3	0.235±0.018	5.4±0.2
Hydrophilic groups	8.5±0.5	0.475±0.011	4.0±0.2
Buffer	∞	0.335	3.9±0.3
		Pyr_2LPC	
Hydrophobic core	8.2±0.1	0.234±0.014	5.0±0.2
Hydrophilic groups	9.5±0.3	0.449±0.005	3.9±0.1
Buffer	∞	0.335	3.4±0.1
		Pyr_3LPC	
Hydrophobic core	8.3±0.4	0.207±0.019	6.1±0.3
Hydrophilic groups	7.9±0.7	0.475±0.019	4.7±0.1
Buffer	∞	0.335	3.7±0.3
		Pyr_4LPC	
Hydrophobic core	8.3±0.3	0.198±0.015	5.5±0.3
Hydrophilic groups	8.6±0.3	0.473±0.011	4.5±0.3
Buffer	∞	0.335	4.0±0.2

4. Discussion

The surface pressure measurements show that all the studied Pl-Por conjugates can form stable films, but they exhibit different π-A isotherm shapes and compressibility moduli depending on

the linker length and the porphyrin chemical structure. All conjugates form more expanded monolayers than the respective free porphyrins. In addition, the monolayer expansion increases monotonically with the linker length. The lower values of compressional modulus of Ph_xLPC compared to Pyr_xLPC and free porphyrins demonstrate that Ph_xLPC molecules exhibit a relatively low degree of condensation. The Langmuir isotherms experiments complemented with Brewster angle microscopy reveal that only Pyr_xLPC compounds can form domains even at low surface pressures. These results unravel the impact of the porphyrin structure on the packing and order of the conjugates in the monolayers. Furthermore, obvious morphological differences between Ph_xLPC and Pyr_xLPC monolayers but also between the individual Pyr_xLPC compounds were observed in the transferred Langmuir-Blodgett films. Therefore, according to these results, we may assume that the type of attached porphyrin controls the compressibility modulus but also whether domains are formed or not. It should also be noticed that the A_{limit} occupied by Ph_xLPC or Pyr_xLPC conjugates (70-80 $Å^2$) is larger than that of monounsaturated phospholipid such as POPC or SOPC (~65 $Å^2$) [5, 32-33]. This larger molecular area can be related either to the presence of the bulky porphyrin moieties aligned with C16 alkyl chain or lying normal to the interface in the vicinity of the phosphatidylcholine headgroup.

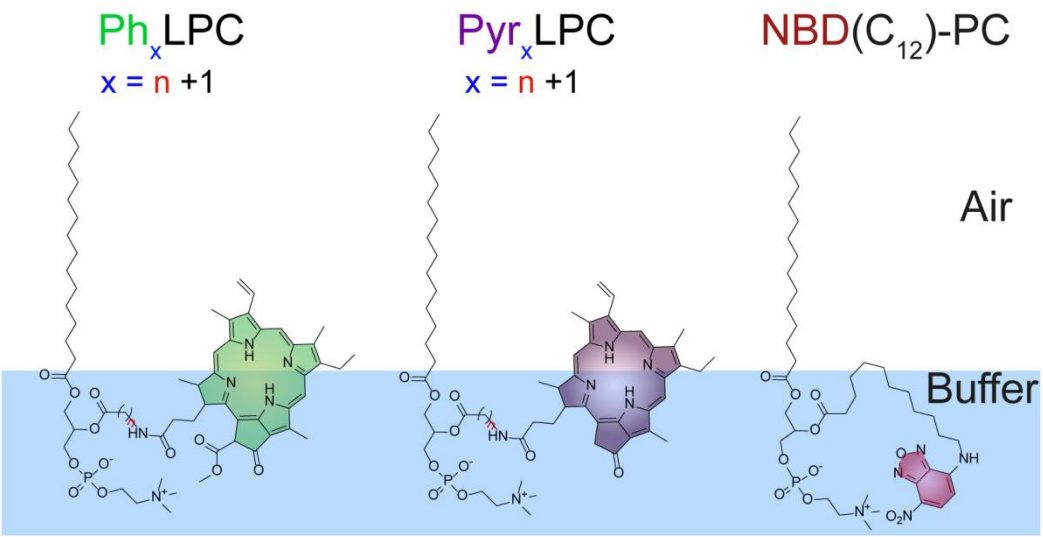

Figure 8 : Schematic illustration of possible orientations of Ph_xLPC and Pyr_xLPC at the air/water interface compared to NBD(C_{12})-PC as described by Tsukanova et al. [29]

Indeed, it was demonstrated by Tsukanova et al. [29] that the monolayer of a chromophore-labeled phospholipid (1-palmitoyl-2-{12-[(7-nitro-2-1,3-benzoxadiazol-4-yl)amino]dodecanoyl}-sn-glycero-3-phosphocholine) named NBD(C_{12})-PC (Figure 8) exhibits LE state with an A_{limit} ~ 80 $Å^2$ similar to A_{limit} for Ph_xLPC and Pyr_xLPC. In addition, their surface potential measurements and spectroscopic data revealed that the NBD group of the NBD-labeled phospholipid embeds into the phospholipid headgroup region. This was attributed to the intermolecular interaction provided by π-cation electrostatic forces between the π-electron of the NBD and the positive charge of the choline group [29]. Porphyrins are π-electron rich moieties; thus, they may interact with the choline group via π-cation as NBD-labeled phospholipids do. To verify such hypothesis, the fine structures perpendicular to the plane of Pl-Por monolayers were analyzed using XRR. The XRR results demonstrated that the porphyrin moieties lie at the air/water interface in both Ph_xLPC and Pyr_xLPC monolayers. Thus π-cation interactions could take place for the Pl-Por conjugates. However, if it is the case then why do Pyr_xLPC compounds form domains and

Ph_xLPC exhibit only less ordered monolayers? One plausible explanation can be drawn from the difference in structure between the Pheo-a and Pyro-a chromophores. In particular the presence of the methyl ester group on the Pheo-a moiety results in two isomers which hinder the lateral packing of molecules and thus, the formation of the condensed monolayers observed for Pyr_xLPC. This is also supported by the slight increase in the A_{limit} of Ph_xLPC compared to Pyr_xLPC (Table 1). Besides, while the porphyrin type allows predicting the formation of domains, the linker length controls their structure and shape. Indeed, the Pyr_2LPC monolayer exhibits a stratified structure with condensed domains, whereas Pyr_3LPC and Pyr_4LPC display predominantly elongated 2D structures where some of them can be piled up into 3D rod-like structures. Although we could not figure out how these compounds are organized within the domains, it can be speculated that changing the number of carbon atoms in the linker gives more flexibility to the attached porphyrin core to adopt different orientations during compression, but it also increases the Van der Waals interactions between the tail groups, promoting the formation of different domain structures.

5. Conclusions

The aim of this work was to assess the impact of the porphyrin structure and chain length separating the polar headgroup from the porphyrin moiety on the interfacial behavior of newly synthesized Pl-Por conjugates (Ph_xLPC and Pyr_xLPC). It was expected that chromophores grafted to a longer chain should align with the sn1 C16 alkyl chain improving the lateral packing properties due to the reduction of the length mismatch between the two chains. Indeed, Carter et al. [34] used molecular dynamics simulations to demonstrate that conjugating a pyro-a derivative (devinyl hexyloxyethy-pyropheophorbide, HPPH) which possesses an hexyl ether moiety at its extremity, enabled the formation of stable bilayers with superior packing properties when

compared to the pyro-a conjugate. Such high packing properties of HPPH-conjugates were related to the hexyl ether moiety which provided a better space filling between the two bilayer leaflets [34]. To verify if a similar behavior can be observed by modulating the chain length between the polar headgroup and the porphyrin moiety, six new Pl-Por conjugates exhibiting different chain lengths in the sn2 position and coupled to 2 different porphyrins, were synthesized and their two-dimensional phase behavior at the air/water interface was studied. Our results revealed that owing to the structural similarities between Pl-Por compounds and conventional phospholipids, Pl-Por conjugates were able to form stable monolayers that were more expanded than those of free porphyrins, due to the presence of the lipid backbone at the interface. Using a variety of physical techniques combined to the Langmuir balance, we demonstrated for the first time that the structure of the porphyrin significantly impacts the lateral packing of the conjugates and controls whether they can form domains or not. Such domains could significantly impact the optical properties and the structure of the supramolecular assemblies made of either pure Pl-Por conjugates or their mixture with conventional phospholipids. Indeed, the presence of such Pl-Por domains in lipid bilayer may favor the formation of J-aggregates that are driven by edge to edge hydrophobic interactions between porphyrin moieties [10-11]. Interestingly, our results revealed for the first time that changing the number of carbon atoms in the linker separating the polar headgroup from the porphyrin core, controls the shape and structure of the organized domains of the conjugates. Although the molecular ordering of these domains could not be determined in this work, other X-ray techniques such as Grazing-incidence small-angle scattering (GISAXS) and Grazing Incidence X-ray Diffraction (GIXD) could be used to get better insight into their fine structure. Whereas GISAXS experiments would enable us to determine the size, the shape parameters as well as the electron density of the crystal domains, the GIXD technique would provide the molecular in-plane organization and the lateral ordering within the domains. Contrary

to our expectations, the XRR results did not show evidence of an alignment between the sn1 and sn2 chains independently of the chain length and porphyrin moiety. This shed light on the importance of π-π interactions between chromophores and π-cations between the chromophore and the choline group in controlling the organization of the Pl-Por conjugates at the air/water interface. Our findings pave the way for future research on the impact of the porphyrin moiety and the structure of polar headgroup on the molecular organization of the conjugates. Finally, although the monolayer study did not reveal an alignment between the two chains, this does not exclude its occurrence in the bilayer assembly. Indeed, the bilayer configuration may promote the inter-leaflet π-stacking between the porphyrin moieties and thus leading to the alignment between the two chains. Hence, this work will be further complemented by bilayer studies to assess the impact of the chemical changes in the Pl-Por conjugates on the structure of their supramolecular assemblies and their optical properties.

CRediT authorship contribution statement

LGB, PC, OK, MJ, WA and AM performed the experiments. LGB, PC, OK, MJ, WA, VR and AM analyzed the data. AM conceptualized, supervised, funded the project and wrote the original manuscript. All the authors reviewed and edited the manuscript.

Declaration of Competing Interest

The authors declare that they have no known competing financial interests or personal relationships that could have appeared to influence the work reported in this paper.

Acknowledgements

LGB is thankful to the French Ministry of Research for the financial support of his PhD thesis. The financial supports for Lipid-Porphyrin conjugates research from the ANR JCJC Grant (Project-ANR-19-CE09-0015), from MITI Auto-organisation 2021 and from the Laboratory of

Excellence LERMIT via an ANR grant (ANR-10-LABX-33) under the program of ‘‘Investissements d’avenir’’ are gratefully acknowledged. We also acknowledge Dr Nada Ibrahim for the fruitful discussion about the porphyrin conjugation protocol.

Appendix A. Supplementary material

References

[1] L.R. Milgrom, The Colours of Life: An Introduction to the Chemistry of Porphyrins and Related Compounds, Oxford University Press, New York, 1997.
[2] J.-Q. Cai, X.-M. Liu, Z.-J. Gao, L.-L. Li, H. Wang, Chlorophylls derivatives: Photophysical properties, assemblies, nanostructures and biomedical applications, Materials Today 45 (2021) 77-92.
[3] P. Krishnamurthy, T. Xie, J.D. Schuetz, The role of transporters in cellular heme and porphyrin homeostasis, Pharmacology & Therapeutics 114(3) (2007) 345-358.
[4] L. Jiang, C.R.R. Gan, J. Gao, X.J. Loh, A Perspective on the Trends and Challenges Facing Porphyrin-Based Anti-Microbial Materials, Small 12(27) (2016) 3609-3644.
[5] J. Massiot, V. Rosilio, N. Ibrahim, A. Yamamoto, V. Nicolas, O. Konovalov, M. Tanaka, A. Makky, Newly Synthesized Lipid–Porphyrin Conjugates: Evaluation of Their Self-Assembling Properties, Their Miscibility with Phospholipids and Their Photodynamic Activity In Vitro, Chemistry – A European Journal 24(72) (2018) 19179-19194.
[6] J. Massiot, V. Rosilio, A. Makky, Photo-triggerable liposomal drug delivery systems: from simple porphyrin insertion in the lipid bilayer towards supramolecular assemblies of lipid–porphyrin conjugates, Journal of Materials Chemistry B 7(11) (2019) 1805-1823.
[7] J.F. Lovell, C.S. Jin, E. Huynh, H. Jin, C. Kim, J.L. Rubinstein, W.C. Chan, W. Cao, L.V. Wang, G. Zheng, Porphysome nanovesicles generated by porphyrin bilayers for use as multimodal biophotonic contrast agents, Nat Mater 10(4) (2011) 324-32.
[8] M.A. Rajora, J.W.H. Lou, G. Zheng, Advancing porphyrin's biomedical utility via supramolecular chemistry, Chem Soc Rev 46(21) (2017) 6433-6469.
[9] F. Würthner, T.E. Kaiser, C.R. Saha-Möller, J-Aggregates: From Serendipitous Discovery to Supramolecular Engineering of Functional Dye Materials, Angewandte Chemie International Edition 50(15) (2011) 3376-3410.
[10] D.M. Charron, G. Yousefalizadeh, H.H. Buzzá, M.A. Rajora, J. Chen, K.G. Stamplecoskie, G. Zheng, Photophysics of J-Aggregating Porphyrin-Lipid Photosensitizers in Liposomes: Impact of Lipid Saturation, Langmuir 36(19) (2020) 5385-5393.
[11] M. Shakiba, K.K. Ng, E. Huynh, H. Chan, D.M. Charron, J. Chen, N. Muhanna, F.S. Foster, B.C. Wilson, G. Zheng, Stable J-aggregation enabled dual photoacoustic and fluorescence nanoparticles for intraoperative cancer imaging, Nanoscale 8(25) (2016) 12618-25.
[12] L. Cui, Q. Lin, C.S. Jin, W. Jiang, H. Huang, L. Ding, N. Muhanna, J.C. Irish, F. Wang, J. Chen, G. Zheng, A PEGylation-Free Biomimetic Porphyrin Nanoplatform for Personalized Cancer Theranostics, ACS Nano 9(4) (2015) 4484-4495.
[13] M.A. Rajora, L. Ding, M. Valic, W. Jiang, M. Overchuk, J. Chen, G. Zheng, Tailored theranostic apolipoprotein E3 porphyrin-lipid nanoparticles target glioblastoma, Chem Sci 8(8) (2017) 5371-5384.
[14] R.J. Paproski, A. Forbrich, E. Huynh, J. Chen, J.D. Lewis, G. Zheng, R.J. Zemp, Porphyrin Nanodroplets: Sub-micrometer Ultrasound and Photoacoustic Contrast Imaging Agents, Small 12(3) (2016) 371-380.

[15] I. Rizvi, G. Obaid, S. Bano, T. Hasan, D. Kessel, Photodynamic therapy: Promoting in vitro efficacy of photodynamic therapy by liposomal formulations of a photosensitizing agent, Lasers Surg Med 50(5) (2018) 499-505.
[16] G. Obaid, W. Jin, S. Bano, D. Kessel, T. Hasan, Nanolipid Formulations of Benzoporphyrin Derivative: Exploring the Dependence of Nanoconstruct Photophysics and Photochemistry on Their Therapeutic Index in Ovarian Cancer Cells, Photochemistry and Photobiology 95(1) (2019) 364-377.
[17] J. Massiot, A. Makky, F. Di Meo, D. Chapron, P. Trouillas, V. Rosilio, Impact of lipid composition and photosensitizer hydrophobicity on the efficiency of light-triggered liposomal release, Physical Chemistry Chemical Physics 19(18) (2017) 11460-11473.
[18] J. Massiot, W. Abuillan, O. Konovalov, A. Makky, Photo-triggerable liposomes based on lipid-porphyrin conjugate and cholesterol combination: Formulation and mechanistic study on monolayers and bilayers, Biochimica et Biophysica Acta (BBA) - Biomembranes 1864(1) (2022) 183812.
[19] R. Rosseto, J. Hajdu, Synthesis of oligo(ethylene glycol) substituted phosphatidylcholines: secretory PLA2-targeted precursors of NSAID prodrugs, Chem Phys Lipids 163(1) (2010) 110-6.
[20] R. Rosseto, J. Hajdu, Synthesis of phospholipids on a glyceric acid scaffold: design and preparation of phospholipase A2 specific substrates, Tetrahedron 70(19) (2014) 3155-3165.
[21] R. Rosseto, J. Hajdu, Peptidophospholipids: synthesis, phospholipase A2 catalyzed hydrolysis, and application to development of phospholipid prodrugs, Chem Phys Lipids 183 (2014) 110-6.
[22] R. Rezakhaniha, A. Agianniotis, J.T.C. Schrauwen, A. Griffa, D. Sage, C.V.C. Bouten, F.N. van de Vosse, M. Unser, N. Stergiopulos, Experimental investigation of collagen waviness and orientation in the arterial adventitia using confocal laser scanning microscopy, Biomechanics and Modeling in Mechanobiology 11(3) (2012) 461-473.
[23] C. Ponchut, J.M. Rigal, J. Clément, E. Papillon, A. Homs, S. Petitdemange, MAXIPIX, a fast readout photon-counting X-ray area detector for synchrotron applications, Journal of Instrumentation 6(01) (2011) C01069-C01069.
[24] W. Abuillan, E. Schneck, A. Korner, K. Brandenburg, T. Gutsmann, T. Gill, A. Vorobiev, O. Konovalov, M. Tanaka, Physical interactions of fish protamine and antisepsis peptide drugs with bacterial membranes revealed by combination of specular x-ray reflectivity and grazing-incidence x-ray fluorescence, Phys Rev E 88(1) (2013) 012705.
[25] A. Nelson, Co-refinement of multiple-contrast neutron/X-ray reflectivity data using MOTOFIT, J Appl Crystallogr 39 (2006) 273-276.
[26] E. Chifu, J. Zsakó, M. Tomoaia-Cotişel, Xanthophyll films: I. Single-component monolayers at the air/water interface, J Colloid Interf Sci 95(2) (1983) 346-354.
[27] M. Jurak, K. Szafran, P. Cea, S. Martín, Analysis of Molecular Interactions between Components in Phospholipid-Immunosuppressant-Antioxidant Mixed Langmuir Films, Langmuir 37(18) (2021) 5601-5616.
[28] O. Albrecht, H. Gruler, E. Sackmann, Polymorphism of phospholipid monolayers, J. Phys. France 39(3) (1978) 301-313.
[29] V. Tsukanova, D.W. Grainger, C. Salesse, Monolayer Behavior of NBD-Labeled Phospholipids at the Air/Water Interface, Langmuir 18(14) (2002) 5539-5550.
[30] J.T. Davies, E.K. Rideal, Interfacial Phenomena, Academic Press: New York and London1963.
[31] J. Daillant, A. Gibaud, X-ray and Neutron Reflectivity: Principles and Applications, Springer-Verlag, Berlin Heidelberg, 2009.
[32] A. Korytowski, W. Abuillan, A. Makky, O. Konovalov, M. Tanaka, Impact of Lipid Oxidization on Vertical Structures and Electrostatics of Phospholipid Monolayers Revealed by Combination of Specular X-ray Reflectivity and Grazing-Incidence X-ray Fluorescence, J Phys Chem B 119(30) (2015) 9787-94.
[33] A. Wnętrzak, K. Łątka, P. Dynarowicz-Łątka, Interactions of Alkylphosphocholines with Model Membranes—The Langmuir Monolayer Study, The Journal of Membrane Biology 246(6) (2013) 453-466.

[34] K.A. Carter, S. Shao, M.I. Hoopes, D. Luo, B. Ahsan, V.M. Grigoryants, W. Song, H. Huang, G. Zhang, R.K. Pandey, J. Geng, B.A. Pfeifer, C.P. Scholes, J. Ortega, M. Karttunen, J.F. Lovell, Porphyrin-phospholipid liposomes permeabilized by near-infrared light, Nat Commun 5 (2014) 3546.